PARAMETRIC STUDY OF SOOT FORMATION IN AN AEROENGINE MODEL COMBUSTOR AT ELEVATED PRESSURES BY LASER-INDUCED INCANDESCENCE: EFFECT OF THE FUEL PHASE

U. Meier[1], C. Hassa[1], K.-P. Geigle[2], O. Lammel[2], P. Kutne[2]
German Aerospace Center,
[1]Institute of Propulsion Technology, Linder Höhe, 51147 Cologne
[2]Institute of Combustion Technology, Pfaffenwaldring 38-40, 70569 Stuttgart
Germany

OVERVIEW

The aim was to study the effect of the fuel phase on soot formation in the specific situation of an aeroengine burner. The experiments were therefore to be performed in an environment resembling real aeroengine conditions as close as possible. It was intended to study the influence of operating conditions separately from flow field and fuel composition effects. Consequently, two sets of experiments were performed with two burners running on liquid and prevaporized kerosene, respectively. The burners were chosen with respect to a maximum possible similarity in terms of size, fuel placement, and internal aerodynamics. Tests with both burners were performed for a set of identical operating conditions. Pressure, air preheat temperature, AFR, and pressure drop across the burner were varied to study the effect of these parameters for both fuel phases. In an initial screening campaign during which the effect of parameter variation was observed qualitatively using video recordings and extracted still images, the accessible parameter range and interesting operating points were identified. In a second stage, soot volume fractions were measured quantitatively for the relevant operating conditions using laser-induced incandescence (LII). These results showed differences of fuel placement between the burners despite their near identical aerodynamics. The swirl imparted radial displacement of the liquid fuel leads to additional dilution and thus partly offsets the higher initial volumetric fuel concentration. The measured peak soot concentrations in the region studied were of the same magnitude for gaseous and liquid fuel. However different tendencies for the effect of the operating conditions on soot formation were observed. Increase of soot with air pressure was less for liquid fuel because of improved atomization at higher pressure. For the same reason the decrease of soot formation with increasing burner pressure drop is more important for liquid fuel. Increasing air preheat temperature gave opposite effects: an increase for gaseous and a decrease for liquid fuel. Here vaporization history and burner aerodynamics combine to reduce soot formation in the investigated operating range. It is planned to modify the liquid burner for similar fuel placement in a follow up study and use LII and LIF simultaneously to study the relation between turbulence structure and soot formation.

1. INTRODUCTION

The success in modelling soot production in practical aeroengine combustors depends to a large extent on the correct description of mixing as stated in [1]. In the complex flow field prevailing in such combustors, the size and location of fuel-rich regions as sources of soot depend on fuel placement and mixing in the case of a gaseous fuel. Since up to this date all aeroengines use liquid fuel, it seems to be worthwhile to inspect the contribution of the liquid phase to the part of the mixing, which is relevant to soot production. For a liquid fuel, additional processes like atomization, dispersion and evaporation become relevant. Each of these processes adds an individual time constant to the formation of fuel-rich soot-forming regions, depending on air-to-fuel ratio (AFR), temperature, pressure, and pressure drop across the burner. The contribution of the second phase to mixing takes place on several length scales: the global movements of the spray caused by inertial and centrifugal forces, the mixing around the droplet caused by the Stefan flow in the boundary layer of the droplet on a microscopic scale and the turbulent dispersion of the droplets, the transport and mixing of fuel vapor caused by the turbulence induced relative motion of the droplets and the particle agglomeration and dispersion phenomena caused by coherent structures of turbulence on a scale of the order of the turbulent macroscale.

Depending on these characteristics, both the amount of soot formed and the regions of soot formation may vary. Therefore, it has to be expected that the soot formation process depends on the operating parameters as well as on the geometric features of the injector in a different way for gaseous and liquid fuel.

2. EXPERIMENTAL SETUP

2.1. Combustor

The tests were performed at the Single Sector Combustor (SSC) facility at the DLR Institute of Propulsion Technology, Cologne. It features large optical access for laser-based diagnostic techniques, while at the same time allowing a wide range of operating conditions, in terms of pressure, preheat temperature, AFR, and pressure loss.

The combustion chamber is schematically shown in FIG. 1. It has a square cross section of 102 x 102 mm^2 and a length of 286 mm. Electrically preheated compressed primary air – shown in yellow – is supplied to the plenum upstream from the combustion chamber through a sonic nozzle, which is used for metering the air mass flow. Additional preheated air is diverted from the primary air supply and guided to the windows for cooling,

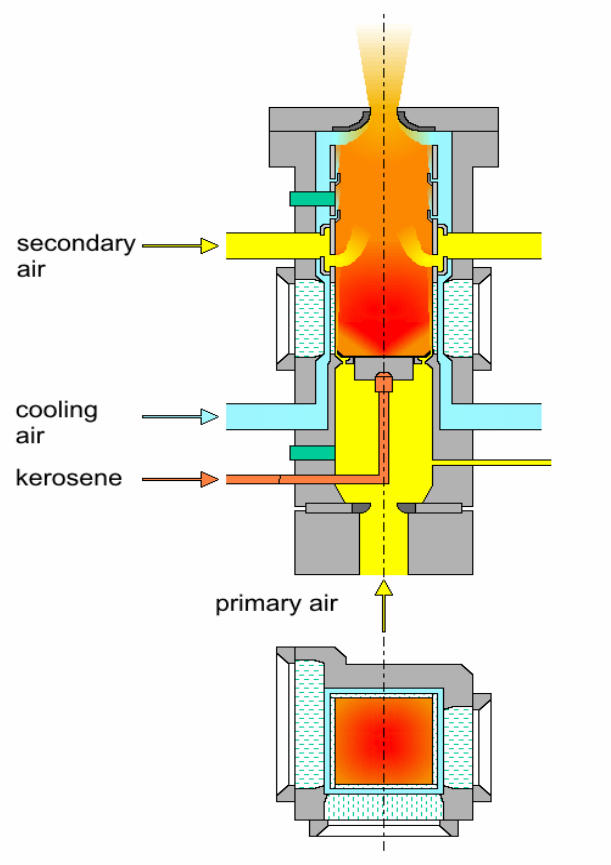

FIG. 1: Schematics of the Single Sector Combustor

and to the downstream section of the flame tube to terminate the recirculation zone of the primary air. All preheated air flows - burner air, window cooling and secondary air - are controlled by sonic nozzles; therefore, the ratios of the air flows are always constant, regardless of the absolute burner air mass flow, which is a function of the variable operating parameters combustor pressure, injector pressure loss and air preheat temperature. According to the sonic nozzle diameters, the mass flow ratio was: burner / window film / secondary air = 1 / 0.53 / 0.80.

The flame tube pressure is controlled by another sonic nozzle forming the choked exit of the combustor, along with additional cooling air (blue) which enters the flame tube just upstream from the exit, after cooling the outside of the windows in the optical section, which extends from 4 to 45 mm distance downstream from the burner faceplate.

The entire rig is mounted on a three-axes traversing stage which allows positioning with respect to the measuring equipment with an accuracy of 0.1 mm. All LII experiments reported here were performed in a plane through the centerline of the fuel injector.

2.2. Fuel injectors

The basic concept of the investigations was to perform measurements with two injectors with a very close resemblance in terms of geometry and aerodynamics, which can be operated on liquid and prevaporized kerosene, respectively. Specifically, the fuel placement for both nozzles should be as similar as possible. Both injectors chosen are based on a design by MTU, with the one used for gaseous fuel modified as shown schematically in the lower part of FIG. 2. In both designs, a sheet of fuel is entrained between an inner and an outer swirling air flow with the same sense of rotation. For liquid kerosene, an airblast nozzle is used, with a pressure atomizer depositing a film of fuel on a prefilmer lip; this film is disintegrated by shear forces at the edge of the prefilmer lip. This injector will hereafter be named “airblast nozzle”. For gaseous kerosene, instead of a prefilmer, an annular slot is used, through which the fuel is fed into the air flow. The slot is separated into 36 channels, each with a cross section of 1.4 x 1.4 mm^2. This nozzle will be referred to as “gas film nozzle”. As an important design criterion, the effective areas and swirl numbers of both burners were closely matched, the effective area being around 200 mm^2.

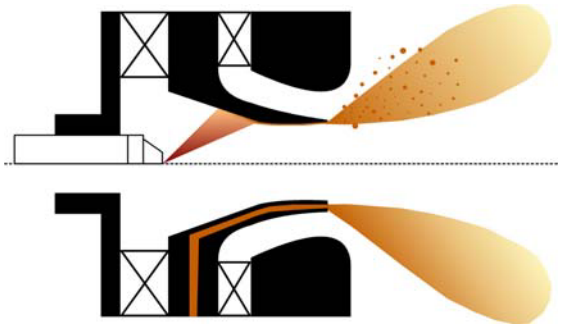

FIG. 2: Schematic representation of the injectors used. Top half: airblast nozzle for liquid fuel; bottom half: gas film nozzle

The swirl vane angles are 60° and 45° for gaseous and liquid fuel, respectively. Taking into account the reduction of the swirl number by the axial momentum of the non-swirling fuel flow of the gas film nozzle, the resulting swirl numbers become comparable.

2.3. Kerosene prevaporizer

Kerosene vapor is generated by a prevaporizer unit. The fuel is vaporized and stored in the isolated, electrically heated tank at 390°C and a pressure of 14 bar. The maximum storage temperature is chosen to prevent the onset of pyrolytic decomposition of kerosene, which starts at about 480°C. This limits the operating pressure of the rig with kerosene vapor to approximately 10 bar. Because kerosene is oxidized by its residual oxygen content at temperatures above 150°C, it is necessary to remove O_2 from the liquid kerosene. This is achieved by evacuating the storage tank and purging it with nitrogen several times. The unit can provide up to 90 kg/h vaporized Jet A-1 fuel at 14 bar feed pressure and a temperature of 390°C.

2.4. Diagnostics

The screening experiments were performed with a JVC TK-C1360B video camera; video sequences were

recorded and stored in digital format using a Hauppauge WinTV-PVR350 analog video grabber. Still images were extracted from the video files.

The LII experiments were performed by the laser diagnostics group at the DLR Institute of Combustion Technology, Stuttgart. Two windows in opposite positions were used for insertion of a laser sheet. The signal is detected under an angle of 90°. In the region of soot production and soot growth two dimensional maps of the local soot concentration were recorded in a plane through the centerline of the burner.

2.4.1. Laser-induced Incandescence

The laser-induced incandescence technique (LII) is based on heating of primary soot particles from flame temperatures up to the vaporisation temperature by a high-energy laser pulse. The absorbed energy is partially emitted as black body radiation with the intensity maximum shifted to the blue compared to the pure flame emission. Above a threshold value in laser power the LII radiation intensity is approximately independent of the laser fluence. Since the particle size is expected to be distinctly smaller than the wavelength of the exciting light (Rayleigh regime) and approximately spherical primary particles can be assumed, the recorded LII signal is directly proportional to the soot volume fraction. For quantification and determination of the calibration factor an independent measurement is necessary (typically an extinction experiment). A comprehensive discussion of the method and its applications can be found in [2] and references therein.

2.4.2. Optical setup

A schematic of the optical setup is shown in FIG. 3. The LII signal was generated using the fundamental of a Nd:YAG laser at 1064 nm. The applied sheet optics (f_{cyl} = -80 mm, f_{sph} = 1000 mm, apertures) produced a light sheet approximately 22 mm wide with a thickness in the order of 200 µm in the probe volume. The complete window section was covered by the measurements by moving the combustor in steps of 15 mm. Because of the abovementioned independence of the LII signal on laser power, as a first approximation a sheet correction procedure was not performed.

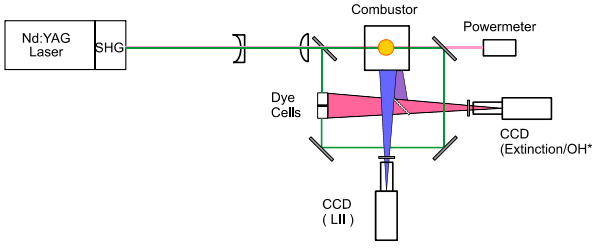

FIG.3: Optical setup of LII diagnostics

LII images were recorded with a gated intensified CCD camera enabling double exposure with a delay being very short compared to the time scale of the turbulence. A first image, taken 500 ns before the LII exciting laser pulse, gave the background of the flame luminosity at the LII detection wavelength of 450 nm. The corresponding single shot LII exposure was started simultaneously with the laser pulse. Both gates were set to 60 ns. Since the flame structures do not change during this short time, the background can be subtracted for each image. The detection volume is limited by the laser sheet thickness and the pixel resolution of the CCD camera being approx. 150 µm. At each burner position and operating point, respectively, 200 images were recorded at a repetition rate of approximately 1 Hz. They cover a detection area of 96 mm x 77 mm, composed of two axial segments due to the limited height of the excitation sheet.

For the calibration of the LII signal a small, temporally relatively stable reference burner implemented into the position of the measurements was used. At this burner an averaged LII image was recorded using the settings of the target experiment. To measure extinction, the laser was operated at 532 nm at low energies to avoid processes other than extinction in the flame. Both beams for LII measurements and calibration by extinction used the same optical pathway. A suitable mirror reflected part of the incident extinction sheet into a quartz cell filled with laser dye. The remaining part of the sheet was partially absorbed by the flame and directed into a second dye cell. The fluorescence from the cells could be imaged by a second camera equipped with a 632 nm interference filter. Since this extinction camera was not required for the target LII measurements of the turbulent flame, it could be used for a complementary measurement: Adding a mirror in front of this second camera and using a 310 +/- 10 nm interference filter, OH chemiluminescence images of the flame were recorded, monitoring qualitatively the line-of-sight integrated reaction zone temporally close to the LII images. Interference of soot luminosity with the LII signal was negligible under the experimental conditions considered here.

2.4.3. Error estimation

Three main sources are responsible for an absolute error of about 40%: the non-uniformity of the used laser profile, the shot to shot fluctuations, and the calibration procedure based on the insufficiently defined optical soot properties. The LII signal intensity is not completely independent of the exciting laser power. Unfortunately, the correlation is not linear and the exact knowledge of the laser power at every point in all three dimensions of the detection volume would be necessary for a proper sheet correction.

Calibration, performed twice during the measurement campaign, resulted in calibration factors varying by about 25%. This might be due to irreproducible pollution of the combustor windows by soot during the extinction measurement. Nevertheless, soot concentrations determined for the spray as well as for the vaporized fuel experiments are qualitatively consistent within their respective phase. General trends in comparing the two different phases of fuel can not be evaluated below this 25% uncertainty.

Systematic errors are signal trapping between the excitation plane and the detector as well as deviations from the assumption of small particles. Because of the small size and relatively low concentrations of soot structures signal trapping should be of minor importance in

this arrangement. For the same reason, a significant attenuation of the exciting laser sheet can be excluded.

3. RESULTS

3.1. Results from the video screening experiments

Videos and photographs give a quick qualitative impression of the position and shape of soot-producing regions in the flame, as well as their dependence on changing operating parameters. Because the LII experiments are time-consuming and generate large amounts of image data, a survey study preceding the LII measurements is most helpful in identifying interesting operating parameters. This procedure is particularly valuable in the case of two different burners, for which a common set of operating conditions has to be found, prior to in-depth investigations using LII.

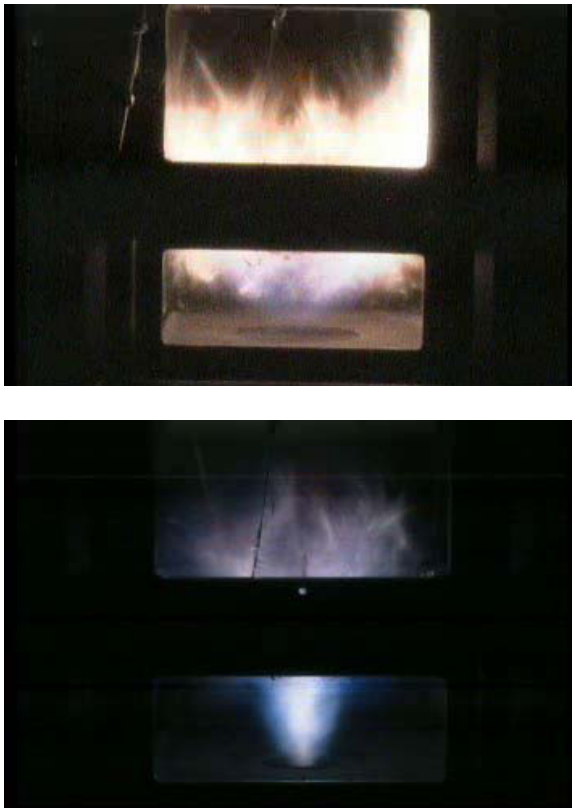

FIG.4: Upper image: liquid kerosene, 500 K preheat temperature; lower image: prevaporized kerosene, 600 K preheat temperature. Combustor pressure 3 bar, AFR 13.8, injector pressure loss 2%

As an example, FIG. 4 shows a comparison of liquid and gaseous kerosene flames under similar operating conditions; the only difference is the higher air preheat temperature in the case of prevaporized kerosene. The wide black horizontal bar near the center of the flame is the shadow of a window frame which divided the optically accessible region into two sections. This separation was necessary because the cooling air film protecting the inner surface of the windows will deteriorate after approximately 40 mm, depending on flame shape and flow conditions. The LII measurements concentrate on the region near the nozzle exit and therefore cover only the lower optical section.

The exposure times for the two images are different, so intensities are not comparable; nevertheless, a considerable difference in terms of flame shape and location of soot forming regions can be observed. The airblast nozzle (top) results in a flame that expands strongly, and high luminosity, indicating soot formation, is found mainly at axial distances above 20 mm from the burner faceplate, and spread over large lateral regions. In contrast, the gas film nozzle (bottom) produces a flame with a rather narrow cone angle; soot production is found mainly near the centerline of the burner and starts immediately at the exit of the injector.

This latter observation can be explained qualitatively, considering additional information available on mixture fraction and flow field of this nozzle, which was obtained in the course of a detailed investigation within the MOLECULES project [3]. First, the flow field of this nozzle is characterized by a pronounced inner recirculation zone. This results in a stabilization of the flame near the nozzle exit by transport of hot reaction products upstream near the centerline of the burner. In addition, measurements of the mixture fraction by Raman scattering [3] show that fuel-rich mixtures are found within this recirculation zone. This means that conditions favorable for soot formation prevail in regions very close to the burner in the case of a gaseous fuel. This consideration illustrates the strong dependence of soot-forming regions, besides kinetic prerequisites, on combustor aerodynamics.

The higher radial expansion of the soot-producing region of the flame fuelled with liquid kerosene, compared to gaseous fuel, is consistently observed for all operating conditions investigated. This is attributed to the effect of dispersion in the presence of droplets, which shifts fuel-rich regions to larger radial positions, as a result of the radial acceleration of droplets in conjunction with the extra time required for evaporation and mixing.

A quick glance at a large number of flames with different operating conditions for both liquid and gaseous fuel led to the definition of a common set of trajectories through parameter space. A reference point, starting from which the four independent parameters pressure, pressure loss, preheat temperature, and AFR were varied, was chosen by the criterion of large changes of observed soot production upon variation of each parameter. It was defined as follows:

Combustor pressure:	9 bar
Injector pressure loss:	3%
Air preheat temperature:	600K
AFR:	14

From this point, all four parameters were varied up and down. The size of the test matrix was limited by different

observations and conditions. For instance, at pressures up to 6 bar, no visible soot production was observed at AFR values above 20 and/or preheat temperature above 700K. Conversely, temperatures below 500K led to stability problems. AFR values below 10 resulted in an unacceptable high thermal load on the combustor walls in the secondary zone, because of the “afterburning” of residual fuel after mixing with the secondary air flow. Combustor pressure was limited to 10 bar, due to the limitation of the prevaporized kerosene feed pressure.

The video still images are qualitatively in good agreement with the LII measurements, beyond that, however, they provide additional information on soot visible further downstream in the upper optical segment of the combustor. This section was not accessible for LII measurements, since although it had an observation window on one side, there were no windows for the laser sheet in this section on the adjacent surfaces. Not surprisingly, the production of soot starts near stoichiometric conditions and increases significantly with decreasing AFR. The soot production zone extends to regions well downstream of the lower optical segment; this has to be kept in mind when interpreting the results of the LII measurements later.

3.2. Results of the LII measurements

In addition to soot volume fraction distributions derived from the LII images, the optical setup provides additional information: The soot luminosity in the spectral window of the LII signals, but in the absence of laser light, is recorded by the double-exposure ICCD camera in a first exposure immediately before the laser pulse. This signal has to be subtracted as background in the course of the data reduction of the LII images. The averaged LII images for the influence of preheat temperature, pressure and pressure loss are compiled in the Figures 5-8 in a representation comparing liquid and gaseous fuel phase.

The time-averaged soot distributions show an asymmetry in the case of gaseous kerosene. This is not a consequence of laser scattering or absorption, but caused by the burner itself, possibly due to a circumferential inhomogeneity of the fuel flow caused by partly clogging of the narrow fuel channels in the annular slot. The soot luminosity images (not shown) exhibit qualitatively the same behavior.

The most striking structural differences of the soot-producing regions for the two phases are the wider cone

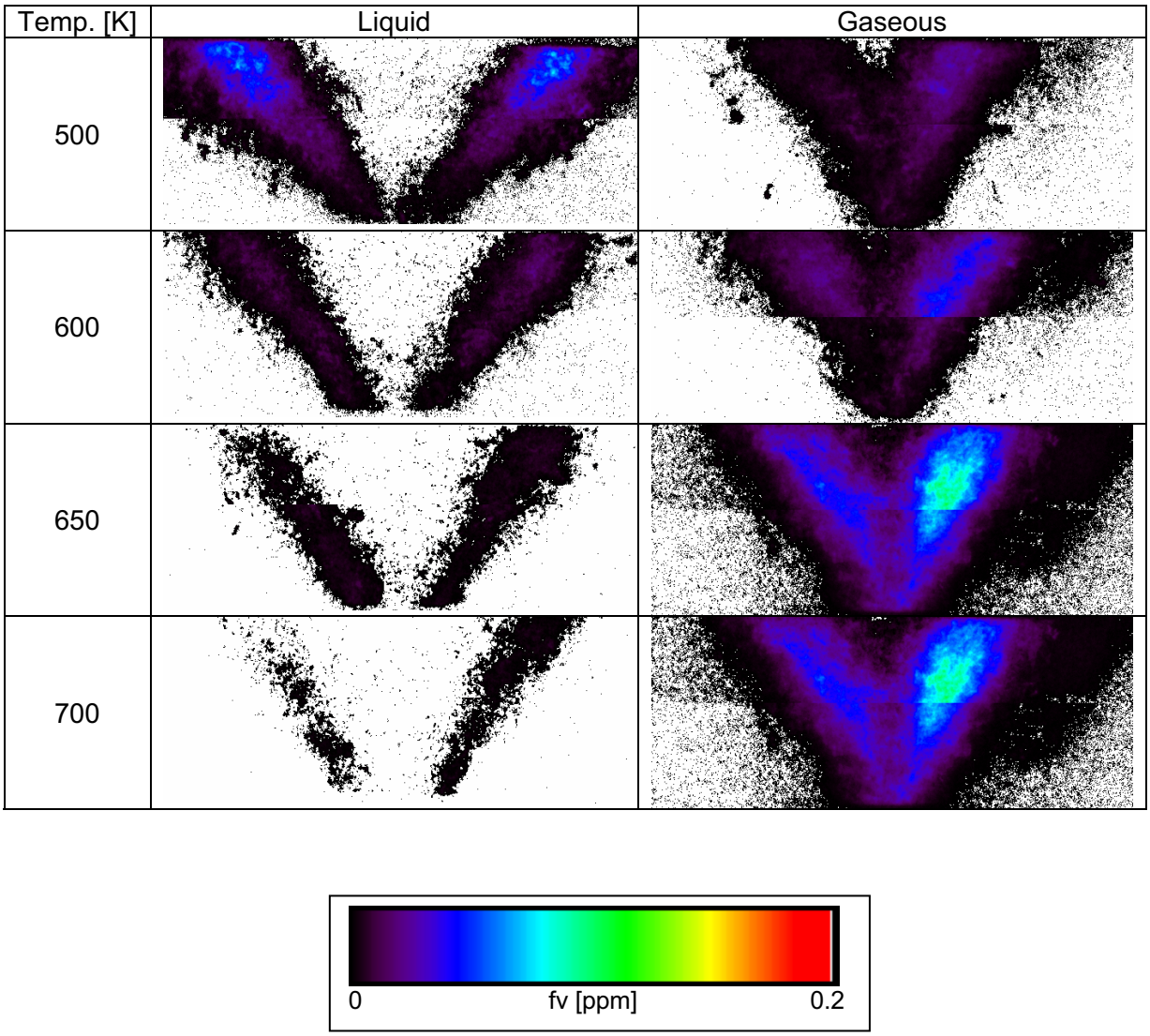

FIG 5: Temperature dependence of average soot volume fractions fv. P = 9 bar, Δp/p = 3%, AFR 14

angle in the case of liquid fuel and the soot formation closer to the burner axis when the fuel is prevaporized. The latter observation and a possible explanation have been discussed in context with the photographs in the previous section. The larger expansion of the flame and the sooting regions, which is clearly visible in both the photographs and the average soot volume distributions derived from LII experiments, is probably a consequence of droplet dispersion: The radial acceleration of the fuel droplets leads to transport of bigger droplets to larger radial distances. Therefore, fuel evaporation and mixing zones are carried further outward, resulting in a shift of heat release also to larger radial distances, which is in agreement with OH chemiluminescence images.

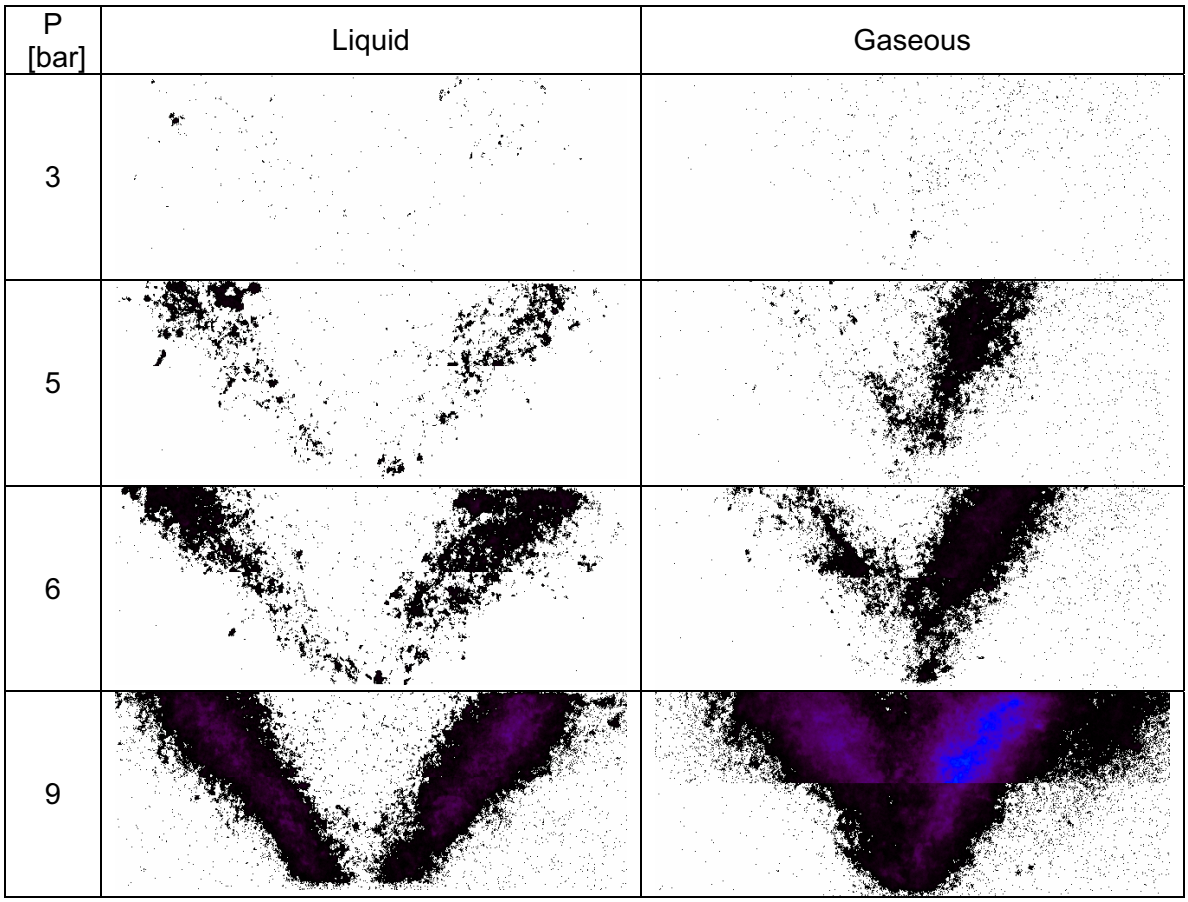

FIG 6: Pressure dependence of average soot volume fractions, T = 600K, $\Delta p/p$ = 3%, AFR 14, color scale as in FIG. 5

It can be seen in Figures 5 to 7 that the measured soot volume fractions are of the same order of magnitude for a given set of operating parameters. On average, soot volume fractions are of the order of 0.1 ppm or less, except at very low burner pressure losses. Furthermore, they follow the same trends with changing operating parameters for liquid and prevaporized kerosene, with one exception: for varying preheat temperatures, the trends are contrary. For gaseous fuel, the soot volume fraction increases with temperature (FIG. 5). This behavior can be expected; it reflects the kinetically controlled dependence of primary soot formation on temperature. In the case of liquid fuel, soot production is closely related to the vaporization rate. As the temperature decreases, vaporization proceeds more slowly compared to mixing, which controls soot formation in the case of a purely gaseous fuel. Common to all swirl burners is a progression of the fuel from a region of high speed and high turbulence to lower values of both. Not common for all spray burners is the amount of flame lift that is exhibited by both of the burners used, which is remarkably stable over the investigated operating conditions. Both features together are responsible for the opposite effect of the preheat temperature variation. As the mixture fraction for the spray burner begins with zero gaseous fuel, a quick vaporization followed by vigorous mixing and hence dilution of the gaseous fuel allows reducing the richness of the mixture before entering the flame zone where all the fuel is quickly vaporized but not mixed as fast. The faster and nearer to the burner the fuel is vaporized, the more time and turbulence intensity of the near burner region goes into premixing. In this way, the liquid burner can avoid soot production at intermediate values of AFR and pressure, where a diffusion burner for gaseous fuel cannot.

A considerable increase of soot volume fraction with pressure is observed for both liquid and gaseous fuel. This can be attributed to an increase of reaction rates for soot

production and was observed experimentally in various laminar flames [5, 6, 7]. At 3 bar, there is hardly any soot observed in the region near the burner (FIG. 6, top row). However, this does not mean that there is no soot produced at all, but merely indicates a kinetically controlled delayed soot formation. At least for liquid fuel there is soot luminosity in the upper optical segment of the combustor at 3 bar - see FIG. 4. Soot volume fractions are very similar for both fuel phases, but their variation with pressure is different. For example, if measurements for 5 and 9 bar are compared (at 3 bar, average volume fractions are too low and their spatial fluctuations too high to allow a reliable evaluation), the increase with pressure in a region of the size 2 x 2 mm^2 around the maximum volume fraction in the respective images is a factor of 7 for liquid fuel and a factor of 14 for gaseous fuel. This suggests that the pressure effect on the droplet size reported for airblast atomizers [8], which results in an improved atomization and therefore faster evaporation and mixing with increasing pressure, appears to compensate part of the kinetically caused soot volume fraction increase at rising pressure.

A similar argument holds for the effect of burner pressure loss. Qualitatively, the dependence of soot volume fractions on pressure loss (FIG. 7) is similar for both liquid and gaseous fuel, although different factors contribute to the influence of Δp/p on soot formation. In the case of gaseous fuel, a larger pressure loss results in higher burner exit velocities, leading to faster mixing and consequently to faster decay of fuel-rich, soot-forming regions. For liquid fuel, the soot formation is additionally affected by the better atomization with increasing pressure loss [8], resulting in smaller droplets and thereby enhanced evaporation and mixing. This may explain the stronger effect of Δp/p in the case of liquid fuel: While the maximum soot volume fraction in the averaged distribution increases for prevaporized kerosene by a factor of 7 when the pressure loss decreases from 3 to 1.5%, it is a factor of 16 for liquid kerosene.

A comparison of soot volume fractions between gaseous and liquid kerosene at various operating parameters shows that, in general, the volume fractions are always lower for liquid fuel under otherwise identical conditions, with the exception of temperature variation discussed earlier. Considering that fuel atomization and evaporation result in a longer persistence of fuel-rich regions, and consequently enhanced soot production, this result comes unexpected. A possible explanation is suggested by FIG. 8: It shows soot distributions for liquid and prevaporized kerosene at a low air preheat temperature, now with a different range of the color coding scheme for clarity. It can be seen that while for gaseous fuel, the soot volume fraction reaches its maximum at about 20 mm

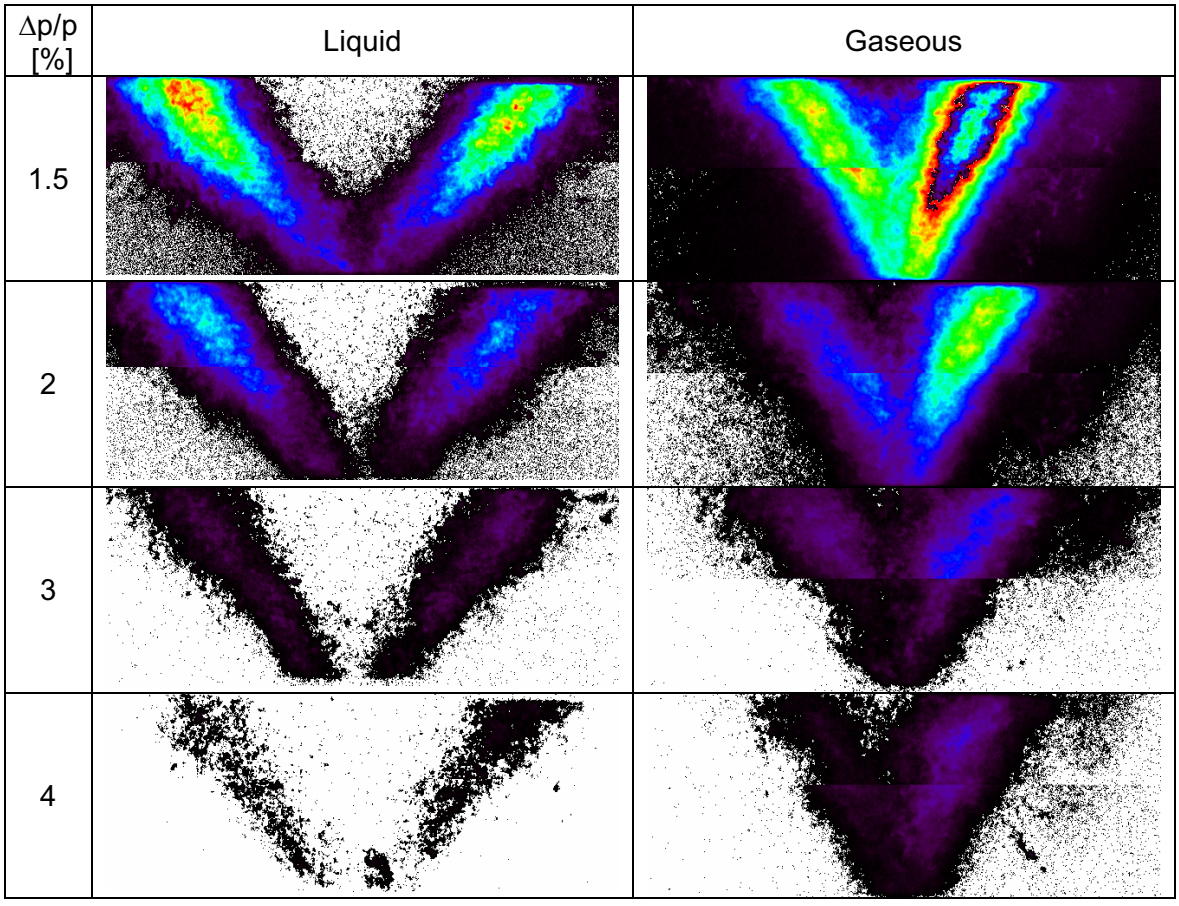

FIG. 7: Pressure loss dependence of average soot volume fractions, T = 600K, p = 9 bar, AFR 14, color scale as in FIG. 5

above the burner exit, in the case of liquid fuel it continues to increase near the edge of the optically accessible region, and possibly beyond. This would mean that the flame running on gaseous fuel may not produce more soot, but produce it earlier. If the occurrence of soot is delayed by the additional time constants resulting from atomization and vaporization, it is conceivable that the maximum of the soot volume fraction is reached too far downstream to be accessible by LII diagnostics in this particular experimental setup. Therefore, it is envisaged to resume the LII experiments with a modified burner/combustor arrangement that would allow tracking a larger part of the history of soot formation at different operating conditions.

made with respect to the frequency of the occurence of the soot clouds. However in the case of gaseous fuel, soot is found more closely to the burner axis. This observation is consistent with time-averaged distributions - see, for example, FIG. 5. Soot appears in distinct clouds with steep gradients at their edges. For both cases, the length scale of the clouds seems to be the same. Shape and location of these clouds are probably correlated with turbulent mixing structure, although this supposition would require as proof a simultaneous experiment for visualization of mixing properties. The images show a considerable temporal fluctuation of the soot clouds, in terms of location, size, and abundance.

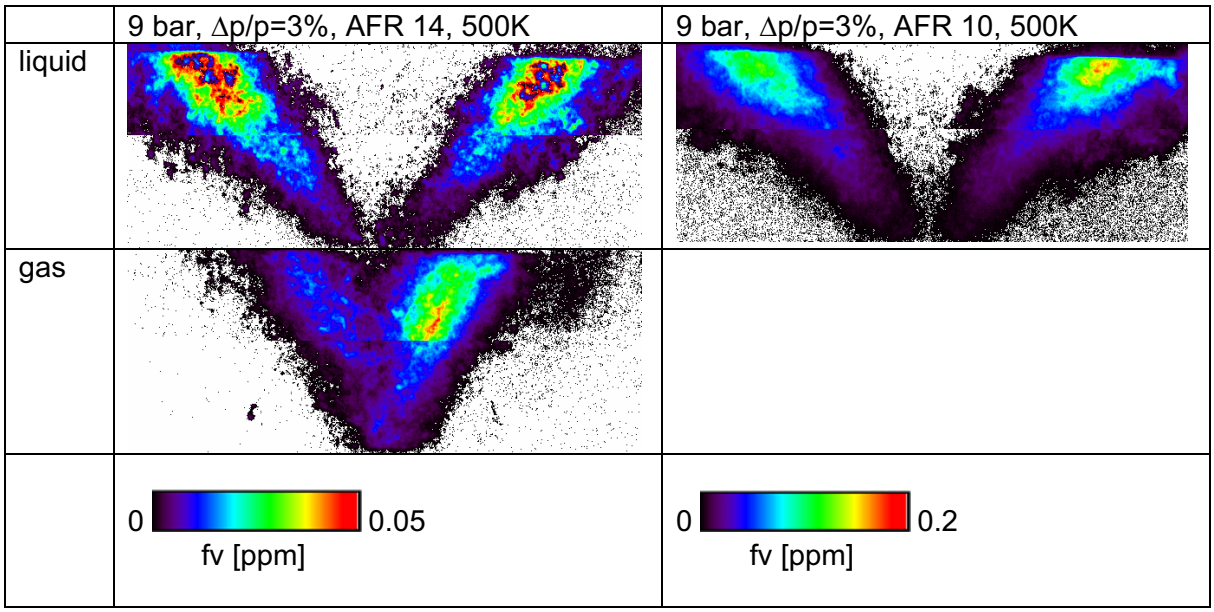

FIG. 8: Average soot volume fraction from liquid and gaseous kerosene at low air preheat temperature

FIG. 9 shows instantaneous soot distributions for liquid and prevaporized kerosene at 9 bar, 3% pressure loss, 500K preheat temperature, and AFR 14. This is the only condition in the test matrix for which the maximum of the average soot volume fraction in the image is comparable for liquid and gaseous fuel. It was chosen to avoid a misleading interpretation of the comparison by significantly larger soot for one fuel phase or the other. In this representation, a false color table different from the one used for average volume fractions is used, in order to give better contrast over a larger range of intensity values covered in the instantaneous images, compared to averages. Nine representative random samples were picked for each phase. Only the upper segment of the field of view, i.e. with the light sheet in the downstream position, between 15 and 35 mm distance from the burner, is shown.

The asymmetry observed in the averaged images also shows up in FIG. 9 for the images of gaseous kerosene. Whereas the right side is comparable to the liquid case, the left side displays fewer structures. As the amount of the inhomogeneity of the fuel distribution is not known, no comparison between liquid and gaseous fuels can be

4. DISCUSSION, CONCLUSIONS AND RECOMMENDATIONS FOR FUTURE WORK

The current experiment was designed to cover the effects of the liquid phase and its vaporization and mixing characteristics down to the turbulent macroscale and indeed it does, but unfortunately some of them are hidden by three drawbacks:

1) Although the swirl of the burners and the acceleration toward the burner mouth was comparable, the heat release of the swirl burner happened further outward due to the radial movement of the spray, which at the same time leads to a dilution of the mixture compared to the gaseous fuel. Hence the mean mixture fractions at the place of heat release, which are not measurable in the experimental situation, are not the same and therefore the different mixing effects of gaseous and liquid fuel are not clearly apparent. What can be said is that for equal soot yields of gaseous and liquid fuel, the soot from liquid fuel is produced in leaner mixtures.

2) The axial length of windows used by LII was not sufficient to cover the soot formation up to its

maximum, especially for the liquid fuel. Due to the unavailability of the originally intended combustor with higher primary zone windows, the shorter version had to be used due to time constraints.

3) The uneven distribution of prevaporized fuel caused asymmetry in the LII images and therefore again an unknown perturbation of the mixture fraction. Due to the highly nonlinear behaviour of the soot formation, this was not recognized on the video images recorded additionally during the measurement for the purpose of monitoring the experiment.

Whereas the first point affects all comparisons in the described manner, the second affects especially situations with higher soot production of the liquid phase as described in the results section, preventing a comparison for low AFR's, lower pressure losses, and the highest pressure level, respectively. The third point affects mostly the comparison of the instantaneous distribution of soot clouds in FIG. 9.

Therefore, it is envisaged to resume the LII experiments with a modified burner/combustor arrangement with lower swirl for the liquid burner leading to a comparable fuel

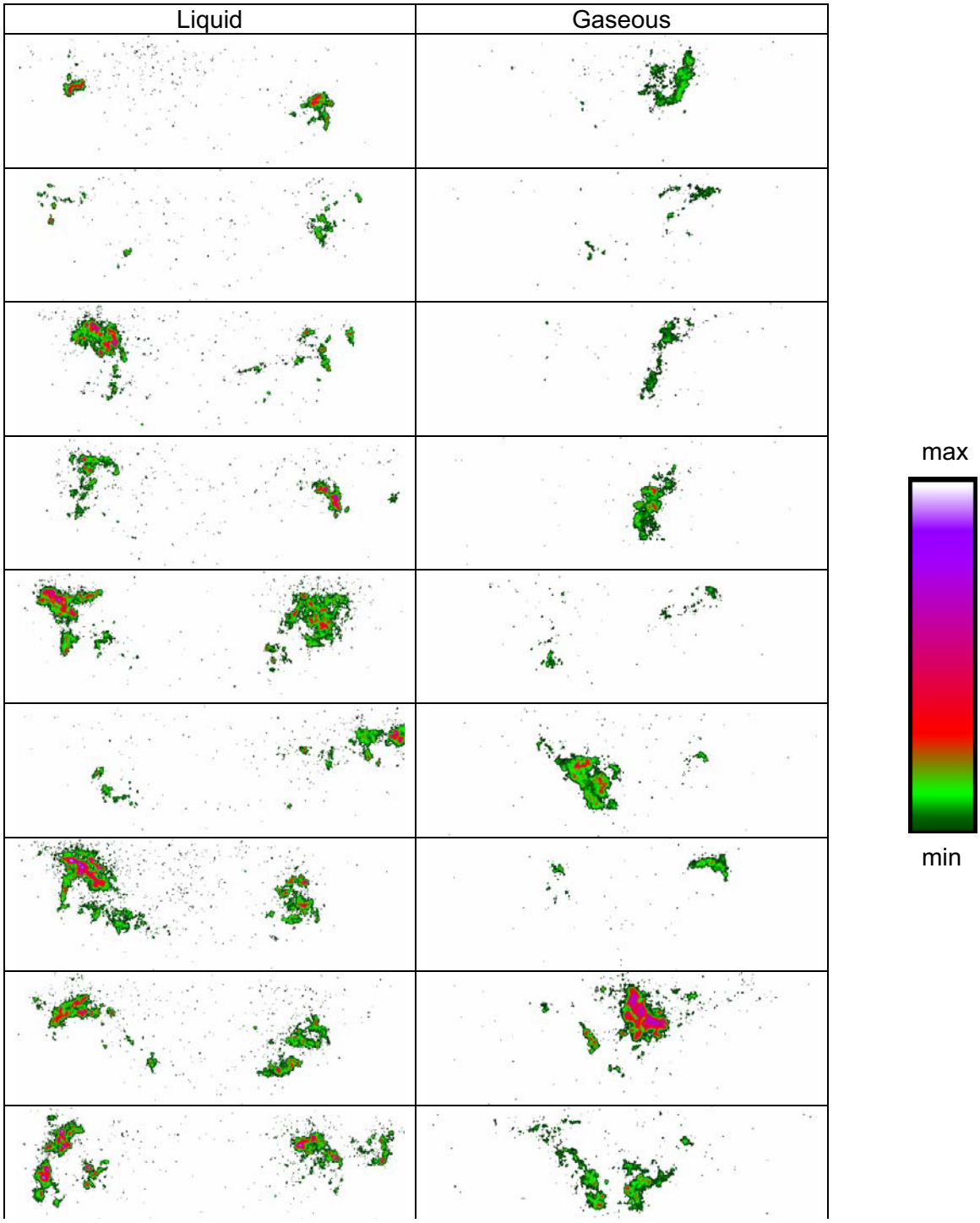

FIG. 9: Instantaneous distributions of soot structures at 9 bar, 3% pressure loss, 500K preheat temperature, and AFR 14. Axial position above burner: 15 to 35 mm downstream of burner exit

placement and a longer primary zone window that would allow tracking a larger part of the history of soot formation at different operating conditions. The measurement routine would have to be changed to allow a quick check of the homogeneity of the fuel distribution of the prevaporized fuel for each day. Finally, to get information about the relation between turbulence structure and soot formation, LII should be complemented with near simultaneous OH-LIF.

The conclusions that nevertheless can be drawn from the results shall now be commented in the light of the aerodynamics of the burners which although they were chosen to be generic, represent one specific class of aeroengine burners.

It has been shown, that the decrease of soot formation with higher preheat temperatures for liquid kerosene depends on the rate of simultaneous vaporization and turbulent mixing of the fuel before it reaches the flame. As it has been pointed out, the effect therefore also depends on the flame lift. Since spray burners all exhibit some degree of lift, the primary zone aerodynamics and specifically the strength of the recirculation decide upon its magnitude. Because most configurations exhibit an inner and outer recirculation zone, it is not surprising that the same tendency has been seen before during an investigation of rich-quench-lean combustion [9].

The pressure and pressure loss effect also depend on the burner aerodynamics. Already for the pressure variation, the amplification of soot production with rising pressure is lower for the liquid burner. For the variation of pressure loss, FIG. 7 shows the soot to almost completely vanish for 4% pressure loss. The stronger effect is caused by the twofold influence of the higher pressure loss to reduce droplet size and increase turbulence near the burner. Therefore it is dependent on the effectiveness with which the energy contained in the burner air flow is coupled into the zone of atomization and dense spray. At the lowest pressure of 3 bar, with the poorest atomization, soot luminosity can be seen in the far field of the liquid burner when the gaseous burner is still blue. This might be explained by the occurrence of single droplet burning of the largest particles of the size distribution, as we have observed a considerable amount of liquid droplets to enter the flame zone in part load situations leading to comparable drop sizes [10].

The comparability of the form and scale of the instantaneous soot clouds underlines the good homogeneity, which can be attained with the pressure swirl atomizer – swirl cup assembly. This is corroborated by the results of a lean blowout study of the same injector showing very sharp blowout values and rather homogeneous flames near blowout [10]. Burners with other injection methods leading to less circumferential homogeneity will probably lead to higher soot production by cluster formation of droplets.

These conclusions drawn from the experiment, some thoughts must be given to their applicability to the real engine environment. Although at elevated pressure, the range of experimental conditions was limited in pressure and AFR mostly by the thermal load exerted on the facility, which is normally used to investigate lean burners. Compared to large turbofans with take off pressure ratios in the range of 40, the peak pressure of the experiment is at intermediate or even low pressure. As the soot production for conventional combustors is mostly a problem at peak load and the additional reduction of dropsize from intermediate to high pressure is not so important, the beneficial effect of smaller dropsizes and higher compressor outlet temperatures at take off will eventually be smaller than the parallel acceleration of chemical kinetics. Most practical burners of single annular rich quench lean combustors will display smaller flame lift and therefore the amount of possible premixing is limited. For very rich primary zones, the simultaneous dependence of the soot formation on rich mixtures and high temperatures limits the penalty of an inhomogeneous mixture as the richest spots will be outside of the rich flammability limit, although this increases with pressure. Summarizing that, the spray effects in rich quench lean combustors of large turbofans will be smaller as seen in the experiment. For pilot injectors of lean burning combustors the situation is different, as the highest load is at intermediate conditions near the staging point and the opportunities for soot oxidation are limited by the lower temperature level of lean combustion.

5. ACKNOWLEDGEMENT

Partial funding of the work by the European Community under ‘Competitive and Sustainable Growth’ Programme (1998-2002), project SiA-TEAM, Contract N°: GRD1-2001-41804 is gratefully acknowledged. Additionally, special thanks are expressed for the excellent support of the test campaign by W. Quade and M. Graben.

6. REFERENCES

[1] Brocklehurst, H., Moss, J.B., Hurley, C.D., Priddin, C.H.: Soot and Radiation Modelling in Gas Turbine Combustion Chambers, RTO Meeting Proceedings 14, Gas Turbine Engine Combustion, Emissions and Alternative Fuels, 1999

[2] Schulz C., Kock B.F., Hofmann M., Michelsen H., Will S., Bougie B., Suntz R., Smallwood G.: Laser-Induced Incandescence: Recent Trends and Current Questions. Appl. Phys. B 83, 333-354, 2006

[3] Hassa, C.; Willert, C.; Fischer, M.; Stockhausen, G.; Röhle, I.; Meier, W.; Wehr, L.; Kutne, P.: Nonintrusive Flowfield, Temperature and Species Measurements on a Generic Aeroengine Combustor at Elevated Pressures. ASME Turbo Expo 2006: Power for Land, Sea and Air, Barcelona, Spain, ASME-GT-90213, 2006

[4] Najm H., Paul P., Mueller C., Wyckhoff P.: On the Adequacy of Certain Experimental Observables as Measurements of Flame Burning Rate. Combust. Flame 113, 312-332, 1998

[5] Wagner, H.G.: The Influence of Pressure on Soot Formation. AGARD Conference Proceedings 422: Combustion and Fuels in Gas Turbine Engines, 24-1, 1988

[6] Tsurikov M.S., Geigle K.P., Krüger V., Schneider-Kühnle Y., Stricker W., Lückerath R., Hadef R., Aigner

M.: Laser-Based Investigation of Soot Formation in Laminar Premixed Flames at Atmospheric and Elevated Pressures. Combustion Science and Technology 177 (10), 1835, 2005

[7] Thomson K.A., Snelling D.R., Smallwood G.J., Liu F.: Laser Induced Incandescence Measurements of Soot Volume Fraction and Effective Particle Size in a Laminar Co-annular Non-premixed Methane/Air Flame at Pressures between 0.5-4.0 MPa. Applied Physics B - Lasers and Optics 83 (3), 469, 2006

[8] Cao M., Eickhoff H, Joos F., Simon B.: Influence of Operating Conditions on the Atomization and Distribution of Fuel by Air Blast Atomizers. AGARD Conference Proceedings 422: Combustion and Fuels in Gas Turbine Engines, 8-1, 1988

[9] Griebel, P., Fischer, M., Hassa, C., Magens, E., Nannen, H., Winandy, A., Chrysostomou, A., Meier, U., Stricker, W.: Experimental Investigation of an Atmospheric Rectangular Rich Quench Lean Combustor Sector for Aeroengines, ASME 97-GT-146, 1997

[10] Hassa, C. Heinze, J., Stursberg, K.: Investigation of an Air Blast Atomizer Combustion Chamber Configuration on Forced Modulation of Air Feed at Realistic Operating Conditions, J. of Eng. for Gas Turbines and Power 125, 872, 2003